Journal of System Design and Dynamics

Vol.4, No.2, 2010

Autonomous Hovering and Landing of a Quad-rotor Micro Aerial Vehicle by Means of on Ground Stereo Vision System*

Dwi PEBRIANTI**, Farid KENDOUL***, Syaril AZRAD**,
Wei WANG*** and Kenzo NONAMI***

** Graduate School of Engineering, Chiba University
1–33 Yayoi cho, Inage ku, Chiba 263–8522, Japan
E-mail: dwi_pebri@graduate.chiba-u.jp

*** Department of Mechanical Engineering, Chiba University
1–33 Yayoi cho, Inage ku, Chiba 263–8522, Japan

Abstract

On ground stereo vision system is used for autonomous hovering and landing of a quad-rotor Micro Aerial Vehicle (MAV). This kind of system has an advantage to support embedded vision system for autonomous hovering and landing, since an embedded vision system occasionally gives inaccurate distance calculation due to either vibration problem or unknown geometry of the landing target. Color based object tracking by using Continuously Adaptive Mean Shift (CAMSHIFT) algorithm was examined. Nonlinear model of quad-rotor MAV and a PID controller were used for autonomous hovering and landing. The result shows that the Camshift based object tracking algorithm has good performance. Additionally, the comparison between the stereo vision system based and GPS based autonomous hovering of a quad-rotor MAV shows that stereo vision system has better performance. The accuracy of the stereo vision system is about 1 meter in the longitudinal and lateral direction when the quad-rotor flies in 6 meters of altitude. In the same experimental condition, the GPS based system accuracy is about 3 meters. Additionally, experiment on autonomous landing gives a reliable result.

Key words : Quad-rotor MAV, Camshift Algorithm, Stereo Vision, Autonomous Hovering, Autonomous Landing

1. Introduction

Research on Unmanned Aerial Vehicles, UAV becomes rapidly increasing since UAV has many advantages not only in the field of military and reconnaissance, but also for applications such as terrain and utilities inspection, disaster monitoring, environmental surveillance, search and rescue, law enforcement and traffic surveillance, communication relay, media services and remote sensing, planetary exploration, agriculture, indoor application and etc.[1].

Many researchers try to broaden the scope of their research not only on UAV but also Micro Aerial Vehicles, MAV. According to the 1st US-Asian Demonstration and Assessment of Micro Air and Unmanned Ground Vehicle Technology, MAV'08 in India, the MAV size is about 30 cm. Such kind of system has some advantages compared to UAV, for example, it can do tasks in a very narrow area such as inside tunnels, buildings, etc. And also, its noise due to motor sounds or rotor rotation is very small. Therefore, for search and rescue task is really appropriate, since the victims voice will not be interfered by MAV noise.

Research on UAV-MAV ranges from system modeling and identification, controller design, sensor integration and hardware implementation. In the term of autonomous flight, there are several tasks that should be conducted, including, taking off, hovering and landing.

Many research on UAV-MAV has been conducted by using vision. For example, works

*Received 1 Oct., 2009 (No. 09-0558)
[DOI: 10.1299/jsdd.4.269]

by Yu[2] and Saripalli[3],[10] were concerning about autonomous landing of a UAV by first tracking a special landing target using vision and then Landing on it. Works done by Eric[6] was successfully in doing autonomous hovering of a UAV over a black object, detecting a special target and detecting opening windows in urban area. Works done by Oohira[7] and Altug[4],[5] were using an outer camera for autonomous hovering and autonomous attitude control of MAVs. They have conducted experiments in an indoor environment. Bao[8] and Ettinger[9] tried to use horizon information for controlling UAV. However, work done by Bao was not completed with real experiment.

As explained above, most research on vision based aerial vehicles are conducted by using UAV as their platforms. Research on vision based autonomous MAV, especially the rotorcraft type is rarely done and mostly the research is conducted in an indoor environment and or a fixed wing type of MAV. This is since MAV, especially rotorcraft which is used in this research, has complex dynamics, nonlinearities and high degree of coupling among control inputs and state variables. MAV behavior is getting relatively unstable and will be more sensitive to disturbance, such as wind gust. Therefore, a reliable and robust controller is needed to be developed. Additionally, the payload of MAV is limited. This makes the selection of sensors that will be used becomes a challenging problem. Light weight sensors are preferable. However, light weight sensor means that the performance of the sensor itself is low, which will make the control design becomes more difficult.

In this research, we investigate the possibility of on ground stereo vision system for autonomous hovering and landing of an MAV for outdoor application. The goal of this research is to support an embedded vision system that occasionally has vibration that makes the distance measurement to the ground becomes inaccurate, which makes the autonomous landing process fail[2]. A precise autonomous landing by using on ground stereo vision system is needed, for example, for autonomous recharging system of an MAV after conducting a certain task or guidance of an MAV to land safely on a ground vehicle or other mother-ship vehicle.

This paper is organized as follows. Section 2 introduces the platform and stereo vision system used in this research. Image processing algorithm for object tracking will be described in Section 3. Section 4 explains about the controller for autonomous hovering and landing of the MAV. Section 5 shows the experimental result and discussion. Conclusion and future works will be expressed in Section 6.

2. MAV Platform and Stereo Vision System

2.1. MAV Platform

The platform used in this research is an off-the-shelf quad-rotor type MAV, X-3D-BL platform from Ascending Technology. Fig.1(a) shows the original platform and Fig.1(b) shows the platform that has been completed with MNAV100CA sensor from Crossbow and Gumstix Connex micro-controller for Flight Control Computer (FCC). The specification of the platform is shown in Table 1.

Table 1 Specification of the platform

Items	Description
Height	200 mm
Diameter	530 mm (with blade)
Mass	400 g (original platform with battery) 600 g (modified platform with battery)
Max. Lift	80 g/f
Max. Payload	plus 300 g of its original weight
Flying Time	23 min (original platform) and 12 min (modified platform)
Max. Speed	10 m/s

This platform was chosen because it is advantageous of light weight, good durability when minor crashes happened, and its high performance in terms of payload and stability required for vision based control.

Gumstix Connex micro-controller with 18 g of weight is used for FCC. For autopilot purpose, we used MNAV100CA sensor from Crossbow, a low cost sensor which contains IMU, GPS and pressure sensor with weight about 35 g, excluding the GPS antenna. It includes 3-axis accelerometers, 3-axis angular rate sensors and 3-axis magnetometers, static pressure (altitude) and dynamic pressure (airspeed) sensors and a GPS receiver module. The AVR micro controller (Atmega32) is mounted on the system in order to interface our autopilot with the original X-3D-BL board, by generating PPM signal when receiving control inputs from the FCC. The PPM interface allows for software interpretation of R/C signals (throttle, pitching/rolling/yawing torques, switch, communication status, GPS data) from MNAV100CA are sent to the Gumstix FCC through the serial port RS-232. Gumstix FCC also receives data (image processing output data) from the Image Processing Computer (IPC) placed on the ground.

2.2. Stereo Vision System

Stereo vision system used in this research is a commercial-off-the-shelf (COTS) product, Bumblebee from Point Grey Research. The specification of this Bumblebee is 1) 12 cm baseline, 2) Resolution up to 1204x768, 3) 15 frame per second (fps) of maximum frame rate, 4) 50° horizontal field of view, 5) IEEE 1394 interface, 6) 375 g of weight and 7) dimension 160 mm x 50 mm x 40 mm. Bumblebee is placed to face upward on the ground and connected to a laptop computer for image processing. This computer will send the 3D position data to quad-rotor MAV through WiFi communication. The complete experimental setup is shown in Fig.2.

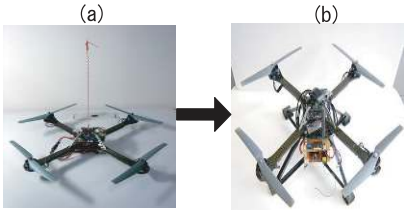

Fig. 1 Quad-rotor MAV

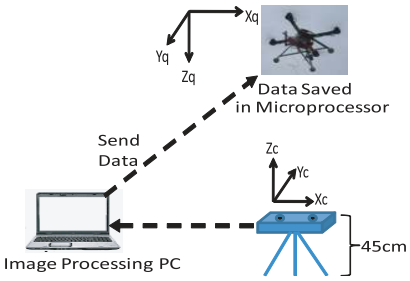

Fig. 2 Experimental Setup

3. Image Processing

3.1. Object Tracking Algorithm : CAMSHIFT

Camshift algorithm was, firstly, developed by Bradski[11]. This algorithm is an application of the mean-shift algorithm for tracking objects in video sequence. The standard mean shift algorithm can only deal with static distributions (i.e., single images) because its search window has a fixed size. Bradski used a dynamic search window that adapts its size after every video frame, depending on the size of the target object.

The step of this algorithm is writen below[12].

(1) Set the region of interest (ROI) of the probability distribution image to the entire image.

(2) Select an initial location of the Mean Shift search window. The selected location is the target distribution to be tracked.

(3) Calculate a color probability distribution of the region centered at the Mean Shift search window.

(4) Iterate Mean Shift algorithm to find the centroid of the probability image. Store the zeroth moment (distribution area) and centroid location.

(5) For the following frame, center the search window at the mean location found in Step (4) and set the window size to a function of the zeroth moment. Go to Step (3).

For further understanding of CAMSHIFT algorithm, reader can refer to G.R. Bradski,

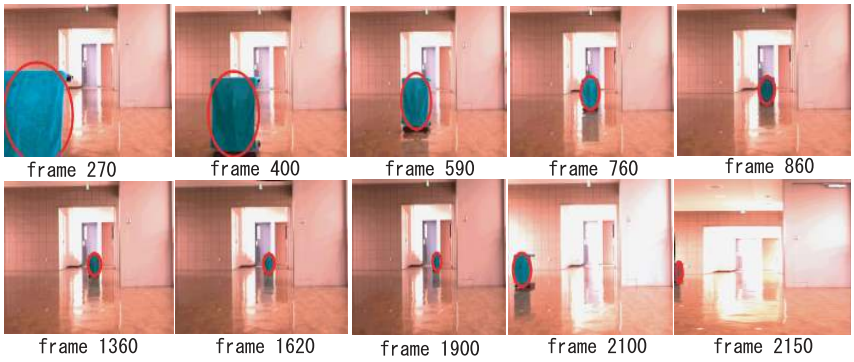

Fig. 3 Result of Object Tracking Using CAMSHIFT Algorithm

"*Computer Vision Face Tracking for Use in a Perceptual User Interface*", Intel Technology Journal, 2, April-June, 1998.

The result of object tracking by using Camshift algorithm is shown in Fig.3.

3.2. 3D Position Calculation

Stereo camera has advantage of ability to measure the 3D position of an object from camera accurately by applying a simple triangle method. The illustration of the 3D position measurement by using a stereo camera is shown in Fig.4.

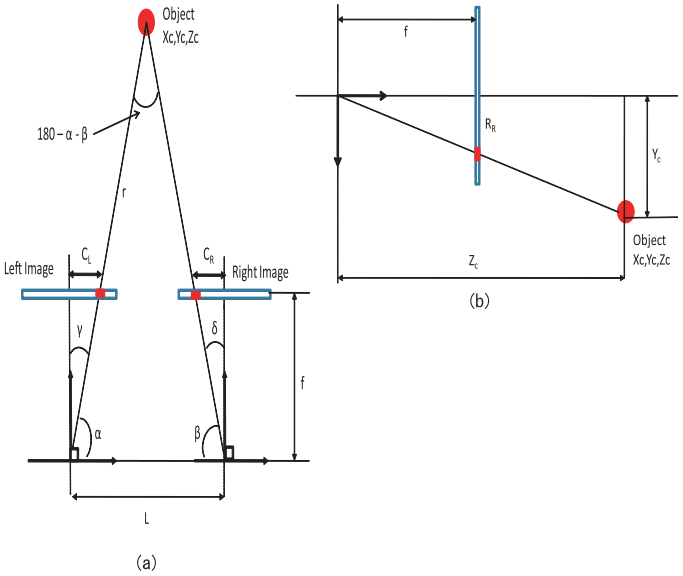

Fig. 4 (a) Configuration between object and image on X-Z plane
(b) Configuration between object and image on Y-Z plane

In Fig.4(a), for finding the values of X_c and Z_c, first we need to derive the relation of the angles by applying Eq.(1).

$$\gamma = \tan^{-1}(\frac{C_L}{f}) \qquad \delta = \tan^{-1}(\frac{C_R}{f})$$
$$\alpha = 90^o - \gamma = 90^o - \tan^{-1}(\frac{C_L}{f}) \qquad \beta = 90^o - \delta = 90^o - \tan^{-1}(\frac{C_R}{f}) \quad (1)$$

By applying sine theorem and using the information of α and β, r can be easily obtained as shown in Eq.(2).

$$r = \frac{L}{\sin(180^o - \alpha - \beta)} \sin(\beta) \quad (2)$$

Therefore, X_c and Z_c of the object from the camera can be expressed by using Eq.(3)

below.

$$X_c = r \cdot \cos(\alpha) \qquad Z_c = r \cdot \sin(\alpha) \tag{3}$$

In order to find the distance on the Y_c direction, Fig.4(b) is used. The Y_c distance is calculated by using Eq.(4).

$$Y_c = Z \cdot \frac{R_R}{f} \tag{4}$$

The 3D position in the camera coordinates is then transformed to the quad-rotor coordinates. The definition of the coordinate system is shown in Fig.2. The matrix transformation from the camera coordinates to the quad-rotor body frame coordinates is expressed in Eq.(5).

$$\begin{bmatrix} \hat{X} \\ \hat{Y} \\ \hat{Z} \end{bmatrix} = \begin{bmatrix} 1 & 0 & 0 \\ 0 & -1 & 0 \\ 0 & 0 & -1 \end{bmatrix} \begin{bmatrix} X_c \\ Y_c \\ Z_c \end{bmatrix} \tag{5}$$

where $[\hat{X}\ \hat{Y}\ \hat{Z}]^T$ and $[X_c\ Y_c\ Z_c]^T$ are 3D position in the quad-rotor body frame coordinates and 3D position in camera coordinates, respectively.

We used Inertial Measurement Unit (IMU) in order to measure the roll, pitch and yaw for attitude control. In the future, we intend to develop attitude control by using a stereo vision camera within short distance, for example, several meters. The range of the distance itself is depending on the size of MAV.

3.3. Kalman Filter

In this research, since we used an on ground stereo vision that gives only 3D position of the quad-rotor, a Kalman filter is applied in order to give velocity estimation for controlling the translational movement of the quad-rotor. Discrete-time Kalman filter equation is shown in Eq.(6) below.

$$\begin{aligned} \mathbf{x}_{k+1} &= F_k \mathbf{x}_k + B_k \mathbf{u}_k + \Upsilon_k \mathbf{w}_k \\ \mathbf{z}_k &= H_k \mathbf{x}_k + \mathbf{v}_k \end{aligned} \tag{6}$$

where $\mathbf{x}_k \in \mathbb{R}^n$ is the state vector, $\mathbf{u}_k \in \mathbb{R}^m$ is the control vector, $\mathbf{w}_k$ is the process noise, $\mathbf{v}_k$ is the measurement noise and $\mathbf{z}_k \in \mathbb{R}^r$ is measured output, all at time k. The state transition matrix, F_k, control distribution matrix, B_k, disturbance matrix, Υ_k and measurement matrix, H_k, are real matrices for appropriate dimensions.

$\mathbf{w}_k$ and $\mathbf{v}_k$ are zero-mean Gaussian white-noise processes, where

$$E(\mathbf{v}_k \mathbf{v}_j^T) = \begin{cases} 0, & k \neq j \\ R_k, & k = j \end{cases} \quad and \quad E(\mathbf{w}_k \mathbf{w}_j^T) = \begin{cases} 0, & k \neq j \\ Q_k, & k = j \end{cases} \tag{7}$$

It is further assumed that $\mathbf{w}_k$ and $\mathbf{v}_k$ are uncorrelated for all k, or $E(\mathbf{v}_k \mathbf{w}_k^T) = 0$. Q_k and R_k are the covariance of process and measurement noise, respectively.

Because the initial condition of the state, $\mathbf{x}_0$, is unknown, the estimation process must begin with an initial guess, or prediction, of the state:

$$\hat{\mathbf{x}}(t_0) = \hat{\mathbf{x}}_0 \tag{8}$$

After an initial time, the estimator will update the current estimation of the state, $\hat{\mathbf{x}}_k$, and to obtain the prediction at the next time step, $\hat{\mathbf{x}}_{k+1}$, based on the measured and estimated output at time k. The estimator works through the dual processes of prediction and update (correction).

The current estimation is first updated (corrected), based on measured and predicted quantities using the update equation :

$$\hat{\mathbf{x}}_k^+ = \underbrace{\hat{\mathbf{x}}_k^-}_{model\ prediction} + \underbrace{K_k[\mathbf{z}_k - H_k \hat{\mathbf{x}}_k^-]}_{residual\ error} \tag{9}$$

where the (ˆ) denotes an estimated quantity and the superscripts − and + denote the predicted state before and after the update.

Once the estimation is updated with Eq.(9), the estimation is propagated forward in time using the model for the system and the known input at time k:

$$\hat{\mathbf{x}}_{k+1}^{-} = F_k \hat{\mathbf{x}}_k^{+} + B_k \mathbf{u}_k \tag{10}$$

This value is then used as the model prediction in the update equation at the next time step, and the process repeats.

Next, we assume an estimation error which is defined as the estimated state minus the true state, as shown in Eq.(11).

$$\tilde{\mathbf{x}}_k = \hat{\mathbf{x}}_k - \mathbf{x}_k \tag{11}$$

The estimation error covariance matrix is defined as the expectation of the squared sum of the estimation errors

$$P_k = E(\tilde{\mathbf{x}}_k \tilde{\mathbf{x}}_k^T) \tag{12}$$

By using Eq.(9) and Eq.(10), the estimation error covariance before and after update is shown in Eq.(13).

$$\begin{aligned} P_k^{+} &= [I - K_k H_k] P_k^{-} \\ P_{k+1}^{-} &= F_k P_k^{+} F_k^T + \Upsilon_k Q_k \Upsilon_k^T \end{aligned} \tag{13}$$

The time-varying gain, K_k, is derived using Eq.(14).

$$K_k = P_k^{-} H_k^T [H_k P_k^{-} H_k^T + R_k]^{-1} \tag{14}$$

We applied 3 Kalman filters for each X, Y and Z direction. For X direction, $\mathbf{x}_k = \begin{bmatrix} x & \dot{x} \end{bmatrix}^T$, for Y direction, $\mathbf{x}_k = \begin{bmatrix} y & \dot{y} \end{bmatrix}^T$, and for Z direction, $\mathbf{x}_k = \begin{bmatrix} z & \dot{z} \end{bmatrix}^T$. The measurement output $\mathbf{z}_k$ is $\hat{X}$, $\hat{Y}$ and $\hat{Z}$ of the quad-rotor obtained from the camera. The control vector $\mathbf{u}_k$ is acceleration on X axis, a_x, acceleration on Y axis, a_y, and acceleration on Z axis, a_z come from the accelerometer. The state transition matrix, F_k is $\begin{bmatrix} 1 & 0.1 \\ 0 & 1 \end{bmatrix}$. The control distribution matrix, B_k is $\begin{bmatrix} 5 \times 10^{-3} \\ 0.1 \end{bmatrix}$. The measurement matrix, H_k is $\begin{bmatrix} 1 & 0 \end{bmatrix}^T$. The covariance of process noise, Q_k is $\begin{bmatrix} 1.25 \times 10^{-5} & 2.25 \times 10^{-4} \\ 2.25 \times 10^{-4} & 5 \times 10^{-3} \end{bmatrix}$. The covariance of measurement noise, R_k is 5×10^{-3}.

4. Mathematical Model and Nonlinear Control

4.1. Quad-rotor Dynamics Modeling

4.1.1. Rigid Body Dynamics In this research, we applied a rigid body dynamics in order to find the model of the quad-rotor MAV. The equation of motion for a rigid body of mass $m \in \mathbb{R}$ and inertia matrix $\boldsymbol{J} \in \mathbb{R}^{3\times3}$ subject to external force $\boldsymbol{F} \in \mathbb{R}^3$ and torque vector $\Gamma^b \in \mathbb{R}^3$ is given by the following Newton-Euler equations, expressed in the body-fixed reference frame $\boldsymbol{B}$.

$$\begin{aligned} m\dot{V} + \Omega \times mV &= \boldsymbol{F} \\ \boldsymbol{J}\dot{\Omega} + \Omega \times \boldsymbol{J}\Omega &= \Gamma^b \end{aligned} \tag{15}$$

where $V = (u,v,w)$ and $\Omega = (p,q,r)$are respectively, the linear and angular velocities in the body-fixed reference frame. The translational force $\boldsymbol{F}$ combines gravity, main thrust and other body force components.

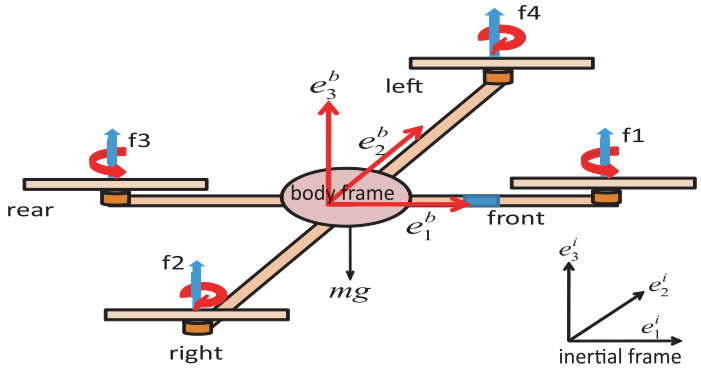

Fig. 5 Rigid Body Dynamics and Associated Frames

Using Euler angles parametrization and "ZYX" convention, the airframe orientation in space is given by a rotation matrix R from $\boldsymbol{B}$ to the inertial reference frame $\boldsymbol{I}$, where $R \epsilon$ SO3 is expressed as follows:

$$\begin{aligned} \mathrm{R} &= R_\psi \cdot R_\theta \cdot R_\phi \\ &= \begin{bmatrix} c\theta\, c\psi & s\phi\, s\theta\, c\psi - c\phi\, s\psi & c\phi\, s\theta\, c\psi + s\phi\, s\psi \\ c\theta\, s\psi & s\phi\, s\theta\, s\psi + c\phi\, c\psi & c\phi\, s\theta\, s\psi - s\phi\, c\psi \\ -s\theta & s\phi\, c\theta & c\phi\, c\theta \end{bmatrix} \end{aligned} \tag{16}$$

where $\eta = (\phi,\theta,\psi)$ denotes the vector of three Euler angles and s., c. are abbreviations for $sin(.)$ and $cos(.)$.

By considering this transformation between the body-fixed reference frame $\boldsymbol{B}$ and the inertia reference frame $\boldsymbol{I}$ as seen in Fig.5. It is possible to separate the gravitational force from other forces and write the translation dynamics in $\boldsymbol{I}$ as follows:

$$\begin{aligned} \dot{\xi} &= \upsilon \\ m\dot{\upsilon} &= R\boldsymbol{F}^b - mge_3^i \end{aligned} \tag{17}$$

where $\xi = (x,y,z)$ and $\upsilon = (\dot{x},\dot{y},\dot{z})$ are the quad-rotor position and velocity in $\boldsymbol{I}$. g is the gravitational acceleration and $\boldsymbol{F}^b$ is the resulting force vector in $\boldsymbol{B}$ (excluding the gravity force) acting on the airframe.

In this research, we used Euler angle parametrization to express rotational dynamics in an appropriate form for control design. The kinematic relation between Ω and $\dot{\eta}$ is expressed by using Eq.(18) written below.

$$\dot{\eta} = \Phi(\eta)\Omega \tag{18}$$

where the Euler matrix $\Phi(\eta)$ is given by

$$\Phi(\eta) = \begin{bmatrix} 1 & sin(\phi)tan(\theta) & cos(\phi)tan(\theta) \\ 0 & cos(\phi) & -sin(\theta) \\ 0 & sin(\phi)sec(\theta) & cos(\phi)sec(\theta) \end{bmatrix} \tag{19}$$

It is important to note that the matrix Φ has a singularity at $\theta = \pm\pi/2$, and its inverse matrix $\Psi(\eta) = \Phi^{-1}(\eta)$ is given by

$$\Psi(\eta) = \begin{bmatrix} 1 & 0 & -sin(\theta) \\ 0 & cos(\phi) & cos(\theta)sin(\phi) \\ 0 & -sin(\phi) & cos(\theta)cos(\phi) \end{bmatrix} \tag{20}$$

By differentiating Eq.(18) with respect to time, and recalling the second equation of Eq.(15), we write

$$\ddot{\eta} = \dot{\Phi}\Omega + \Phi\dot{\Omega} = \dot{\Phi}\Psi\dot{\eta} - \Phi\boldsymbol{J}^{-1}sk(\Omega)\boldsymbol{J}\Omega + \Phi\boldsymbol{J}^{-1}\Gamma^b \tag{21}$$

The *sk* operation is defined here from $\mathbb{R}^3$ to $\mathbb{R}^{3\times3}$ such that *sk*(x) is a skew-symmetric matrix associated to the vector product *sk*(x)y := x × y for any vector y ϵ $\mathbb{R}^3$.

By multiplying both sides of the last equation by $\mathrm{M}(\eta) = \Psi(\eta)^T \boldsymbol{J} \Psi(\eta)$, we obtain

$$M(\eta)\ddot{\eta} + C(\eta,\dot{\eta})\dot{\eta} = \Psi(\eta)\Gamma^b \tag{22}$$

with $M(\eta)$ is a well defined positive inertia matrix, provided that $\theta \neq k\pi/2$. The *Coriolis* term $C(\eta,\dot{\eta})$ is given by

$$C(\eta,\dot{\eta}) = -\Psi(\eta)^T \boldsymbol{J} \Psi(\eta) + \Psi(\eta)^T sk(\Psi(\eta)\dot{\eta}) \boldsymbol{J} \Psi(\eta) \tag{23}$$

Thus, the quad-rotor nonlinear model, used for flight controller design, is

$$\begin{aligned} m\ddot{\xi} &= R\boldsymbol{F}^b - mge_3^i \\ M(\eta)\ddot{\eta} + C(\eta,\dot{\eta})\dot{\eta} &= \Psi(\eta)^T \Gamma^b \end{aligned} \tag{24}$$

4.1.2. Aerodynamics Forces and Toques Quad-rotor MAV can be characterized by three main control torques $\tau = (\tau_\phi, \tau_\theta, \tau_\psi)^T$ and one main control force $\boldsymbol{F}^b = (0,0,u)^T$. The four control inputs $(u, \tau_\phi, \tau_\theta, \tau_\psi)$ are obtained by independently controlling the rotation speed of each motor. The collective lift u is the sum of the thrusts generated by the four propellers.

$$u = \sum_{i=1}^{4} f_i \tag{25}$$

The airframe torques generated by rotors are given by[14]

$$\tau_\phi = l(f_2 - f_4) \tag{26}$$

$$\tau_\theta = l(f_3 - f_1) \tag{27}$$

$$\tau_\psi = Q_1 + Q_3 - Q_2 - Q_4 \tag{28}$$

l represents the distance from the rotors to the center of mass of the helicopter and Q_i is the fan torque due to air drag.

Propellers thrust and torque are generally assumed to be proportional to the square of the rotor angular velocity ω. In fact, the relations between the rotor speed w_i and the generated lift f_i and torque Q_i are very complex[15],[16]. Therefore, the algebraic model for generating the force and control torques can be written in the following form:

$$\begin{bmatrix} u \\ \tau_\phi \\ \tau_\theta \\ \tau_\psi \end{bmatrix} = \begin{bmatrix} \rho & \rho & \rho & \rho \\ 0 & -l\rho & 0 & l\rho \\ -l\rho & 0 & l\rho & 0 \\ \kappa & -\kappa & \kappa & -\kappa \end{bmatrix} \begin{bmatrix} w_1^2 \\ w_2^2 \\ w_3^2 \\ w_4^2 \end{bmatrix} \tag{29}$$

where (ρ,κ) are positive constants characterizing the propeller aerodynamics. The expressions in Eq.(29) are valid approximations that are used in cases of hovering and low-speed displacements.

The dynamical model, considered for quad-rotor control design is given by the following Eq.(30):

$$\begin{aligned} m\ddot{\xi} &= uRe_3^i - mge_3^i \\ M(\eta)\ddot{\eta} + C(\eta,\dot{\eta})\dot{\eta} &= \Psi(\eta)^T \tau \end{aligned} \tag{30}$$

4.2. Controller Design

The controller used here is a hierarchical flight controller that exploits the structural properties of the quad-rotor model given by Eq.(30).

The aircraft model is separated into two connected subsystems by decoupling the translational dynamics (outer-loop) and rotational dynamics (innerloop). The time-scale separation

between the two subsystems is made by considering the following transformations (or change of variables)[17]:

$$\mu = \frac{1}{m} uR(\phi_d, \theta_d, \psi_d)e_3^i - ge_3^i$$
$$\tau = \boldsymbol{J}\Psi(\eta)\tilde{\tau} + \Psi^{-1}C(\eta, \dot{\eta})\dot{\eta} \quad (31)$$

where $\tilde{\tau}$ is a new torque vector, μ is an intermediary force vector and (ϕ_d, θ_d, ψ_d) are desired roll, pitch and yaw angles.

From Eq.(31) above, we can calculate the desired force vector magnitude and desired attitude (θ_d and ϕ_d, in case of ψ_d is given by the user), $(u,\phi_d,\theta_d) = \tilde{\mathfrak{f}}^{-1}(\mu_x, \mu_y, \mu_z)$, that is

$$u = m\sqrt{\mu_x^2 + \mu_y^2 + (\mu_z + g)^2}$$
$$\phi_d = sin^{-1}(m\frac{\mu_x sin\psi_d - \mu_y cos\psi_d}{u})$$
$$\theta_d = tan^{-1}(\frac{\mu_x cos\psi_d + \mu_y sin\psi_d}{\mu_z + g}) \quad (32)$$

By defining the tracking errors $\mathfrak{X} = (\xi - \xi_d, \upsilon - \upsilon_d)^T \in \mathbb{R}^6$ and $e = (\eta - \eta_d, \dot{\eta} - \dot{\eta}_d)^T \in \mathbb{R}^6$, replacing η by $(\eta_d + e)$ in Eq.(30) and considering Eq.(31), the system in Eq.(30) can be written in the following form[17]

$$\dot{\mathfrak{X}} = \underbrace{A_1\mathfrak{X} + B_1(\mu - \ddot{\xi}_d)}_{f(\mathfrak{X},\mu,\ddot{\xi}_d)} + \underbrace{\frac{1}{m}uH(\eta_d, e_\eta)}_{\Delta(u,\eta_d,e_\eta)}$$
$$\dot{e} = A_2 e + B_2(\tilde{\tau} - \ddot{\eta}_d) \quad (33)$$

where $H(\eta_d,e_\eta) = (0, 0, 0, h_x, h_y, h_z)^T$ is a nonlinear connection term. The matrices $A_1 \in R^{6\times6}$, $B_1 \in R^{6\times3}$, $A_2 \in R^{6\times6}$ and $B_2 \in R^{6\times3}$ are defined below.

$$A_1 = A_2 = \begin{bmatrix} 0 & 0 & 0 & 1 & 0 & 0 \\ 0 & 0 & 0 & 0 & 1 & 0 \\ 0 & 0 & 0 & 0 & 0 & 1 \\ 0 & 0 & 0 & 0 & 0 & 0 \\ 0 & 0 & 0 & 0 & 0 & 0 \\ 0 & 0 & 0 & 0 & 0 & 0 \end{bmatrix}, B_1 = B_2 = \begin{bmatrix} 0 & 0 & 0 \\ 0 & 0 & 0 \\ 0 & 0 & 0 \\ 1 & 0 & 0 \\ 0 & 1 & 0 \\ 0 & 0 & 1 \end{bmatrix} \quad (34)$$

The quad-rotor control problem is thus, formulated as the control of two linear subsystems, which are coupled by a nonlinear term $\Delta(u, \eta_d, e_\eta)$. It can be controlled using partially or fully passivation design[18].

Here, we use partial passivation design to synthesize two stabilizing feedbacks $\mu = \alpha(\mathfrak{X}, \ddot{\xi}_d)$, $\tilde{\tau} = \beta(e, \ddot{\eta}_d)$ such that the tracking errors ($\mathfrak{X}$, e) are asymptotically stable for all initial conditions. The idea is to consider $\Delta(u, \eta_d, e_\eta)$ as a disturbance on the $\mathfrak{X}$-subsystem which must be driven to zero, and stabilize independently the $\mathfrak{X}$ and e-subsystems.

Since the $\mathfrak{X}$-subsystem without the coupling $\Delta(.)$ and the e-subsystem in Eq.(33) are linear, we can use simple linear controllers such as PD or PID. Therefore, we synthesize two control laws

$$\mu = -K_{\mathfrak{X}}\mathfrak{X} + \ddot{\xi}_d, K_{\mathfrak{X}} \epsilon \mathbb{R}^{3\times6}$$
$$\tilde{\tau} = -K_e e + \ddot{\eta}_d, K_e \epsilon \mathbb{R}^{3\times6} \quad (35)$$

such that the matrices $A_{\mathfrak{X}} = A_1 - B_1K_{\mathfrak{X}}$ and $A_e = A_2 - B_2K_e$ are Hurwitz.

By substituting Eq.(35) into Eq.(33), the close loop system is given by Eq.(36) below.

$$\dot{\mathfrak{X}} = A_{\mathfrak{X}}\mathfrak{X} + \Delta(\mathfrak{X}, e_\eta)$$
$$\dot{e} = A_e e \quad (36)$$

It is important to note that the control $\mu(\mathfrak{X})$ is computed using the 3D position obtained from stereo vision and velocity predicted by Kalman filter. Indeed, $\mathfrak{X} = (\xi - \xi_d, \upsilon - \upsilon_d)^T$ where $\xi = (\hat{X}, \hat{Y}, \hat{Z})^T$ and $\upsilon = (\hat{V}_X, \hat{V}_Y, \hat{V}_Z)^T$.

Kendoul[13] showed the analysis of the close loop system stability.

In the real implementation, the control laws in Eq.(35) have been slightly modified to include an integral term, thereby increasing the tracking accuracy.

$$\begin{aligned}
\mu_x &= -k_{p_x}(\hat{X} - \hat{X}_d) - k_{i_x}\int(\hat{X} - \hat{X}_d)dt - k_{d_x}(\hat{V}_X - \hat{V}_{X_d}) \\
\mu_y &= -k_{p_y}(\hat{Y} - \hat{Y}_d) - k_{i_y}\int(\hat{Y} - \hat{Y}_d)dt - k_{d_y}(\hat{V}_Y - \hat{V}_{Y_d}) \\
\mu_z &= -k_{p_z}(\hat{Z} - \hat{Z}_d) - k_{i_z}\int(\hat{Z} - \hat{Z}_d)dt - k_{d_z}(\hat{V}_Z - \hat{V}_{Z_d})
\end{aligned} \tag{37}$$

By using Eq.(37) above, total thrust (u) and the desired attitude(ϕ_d, θ_d) can be derived by using Eq.(32).

Then by using this total thrust and desired attitude, the control law for inner loop can be derived, as seen in Eq.(38).

$$\begin{aligned}
\tilde{\tau_\phi} &= -k_{p_\phi}(\phi - \phi_d) - k_{i_\phi}\int(\phi - \phi_d)dt - k_{d_\phi}(\dot{\phi} - \dot{\phi}_d) \\
\tilde{\tau_\theta} &= -k_{p_\theta}(\theta - \theta_d) - k_{i_\theta}\int(\theta - \theta_d)dt - k_{d_\theta}(\dot{\theta} - \dot{\theta}_d) \\
\tilde{\tau_\psi} &= -k_{p_\psi}(\psi - \psi_d) - k_{i_\psi}\int(\psi - \psi_d)dt - k_{d_\psi}(\dot{\psi} - \dot{\psi}_d)
\end{aligned} \tag{38}$$

Parameters used in the experiment are listed in Table.2.

Table 2 Controller gain used in experiment

Parameters	Value		Parameter	Value
k_{p_x}, k_{p_y}	0.8		k_{p_ϕ}, k_{p_θ}	28.0
k_{i_x}, k_{i_y}	0.02		k_{i_ϕ}, k_{i_θ}	0.5
k_{d_x}, k_{d_y}	1.0		k_{d_ϕ}, k_{d_θ}	1
k_{p_x}, k_{p_y}	0.8		k_{p_ϕ}, k_{p_θ}	28.0
k_{p_z}	0.2		k_{p_ψ}	3.0
k_{i_z}	0.02		k_{i_ψ}	0.05
k_{d_z}	0.6		k_{d_ψ}	0.2

The overall diagram of the designed controller is shown in Fig.6.

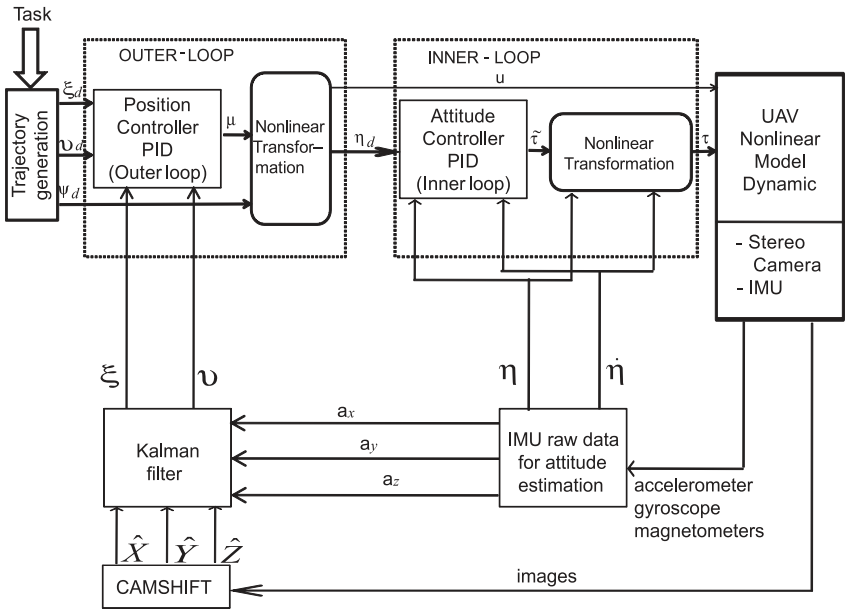

Fig. 6 Structure of the inner-outer loop-based controller

5. Experimental Result and Discussion

5.1. Autonomous Hovering along X,Y and Z axis

In order to evaluate the performance of CAMSHIFT object tracking and the performance of the whole system including the distance measurement by using a stereo vision system and the controller, we have performed real-time flight test for two scenarios. First was to do autonomous hovering and the second one was autonomous landing. The experiment was conducted outdoor on the same day for the two experiments. The weather condition was sunny with wind speed about 3 - 4 m/s.

The procedure of the experiment was first to fly the quad-rotor manually. When it was detected by stereo camera, user selected the quad-rotor and the CAMSHIFT algorithm started. When the CAMSHIFT based object tracking started, the flight mode was changed from manually to autonomous. The reference point for autonomous hovering is the same as the position when we changed the flight mode from manually to autonomous. In this case, we expect that the position reference in the X and Y directions will be 0, since the quad-rotor is in hovering mode and the altitude reference will be the last value obtained from the stereo vision system. In our autonomous hovering experiment, the altitude reference was recorded to be about 6 m. For comparison purpose, the data from GPS and pressure sensor were also recorded.

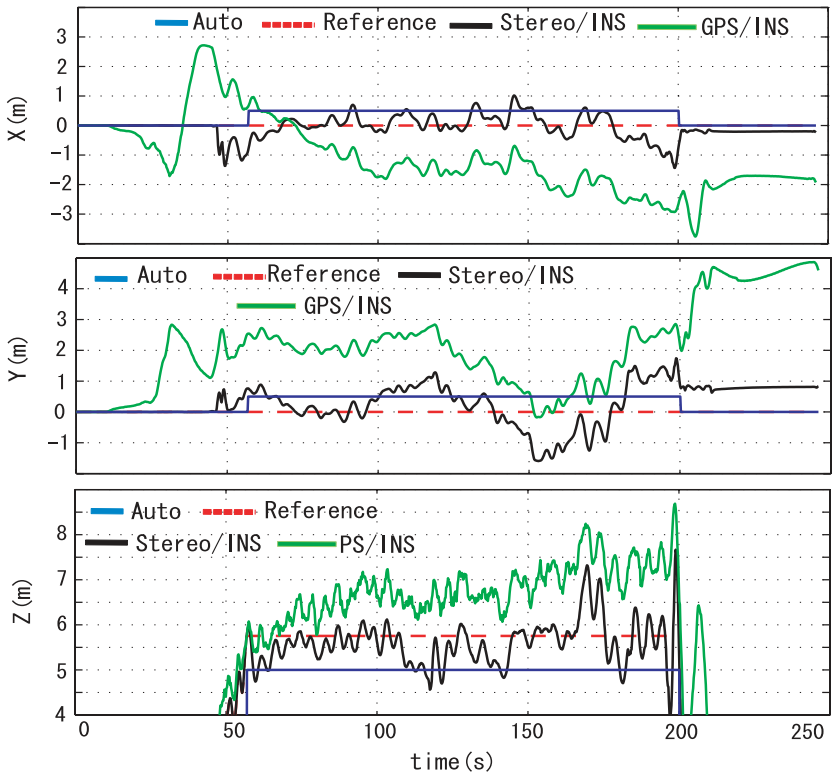

Fig. 7 Quad-rotor Position During Autonomous Hovering

The results of the X, Y and Z positions are shown in Fig.7. As shown in Fig.7 (Top), for longitudinal direction or X axis, the stereo with INS system has accuracy about 1 m when quad-rotor flew about 6 m. On the other hand, GPS has accuracy about 3 - 4 m when quad-rotor flew in the same height. For lateral direction, Y axis, stereo with INS system has accuracy about less than 2 m and the value does not have a big error compared to the reference point. In case of GPS, the accuracy on Y direction is about 3 m.

Moreover, by eye investigation, it was seen that the movements of the quad-rotor along X axis and Y axis were not changing much, which proved that the performance of stereo with INS system is better than GPS.

In case of Z position, as seen in Fig.7 (Bottom), pressure sensor is drifting. In case of altitude from stereo with INS, the value is stable around 6 m, even though it has some oscillation. The oscillation itself is about 1 m. Here, also we can conclude that the performance of stereo vision system is better than pressure sensor. This is true since pressure sensor is influenced easily by wind condition.

Fig.8 shows the velocities along X,Y and Z axis obtained from stereo with INS and GPS. For both systems, the values of velocities are near to the reference point, 0 m/s. From these results we can know that our designed Kalman filter which was used for estimating the velocity by fusing the data of acceleration obtained from INS and positions data from stereo camera has good performance. Velocity sensors on GPS for longitudinal and lateral directions are known to have good performance. As seen in Fig.8 (Top) and (Middle), the velocities obtained from Kalman filter and the velocities came from GPS have more or less the same value.

However, in case of velocity on Z axis, since data obtained from pressure sensor is known to be noisy due to wind as disturbance, when we compared velocity from stereo with INS system with velocity from pressure sensor, we cannot conclude the performance of Kalman filter for Z axis. However, since for Z position, stereo with INS system was used in the control loop, and by eye investigation it was seen that the quad-rotor was very stable even though there was wind for about 3 - 4 m/s, we can conclude that the performance of Kalman filter for Z axis is also good.

Fig.9 shows the attitude of the quad-rotor during autonomous hovering. As we can see here, the roll and pitch angles are less than 10° of movement. It shows that the attitude controller worked well for autonomous hovering. In case of yaw angle, the movement is significant due to sensor problem.

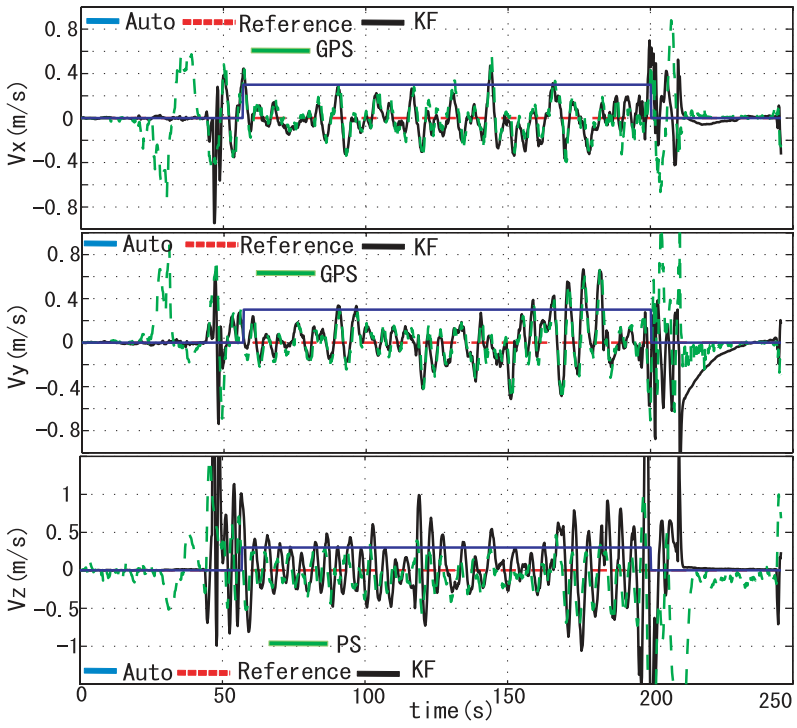

Fig. 8 Quad-rotor Translational Velocities During Autonomous Hovering

5.2. Autonomous Landing

Autonomous landing is one of the tasks that should be achieved by autonomous UAV - MAV[(2)]. Here, we investigated the possibility of autonomous landing for our quad-rotor MAV with nonlinear model by on ground stereo vision system.

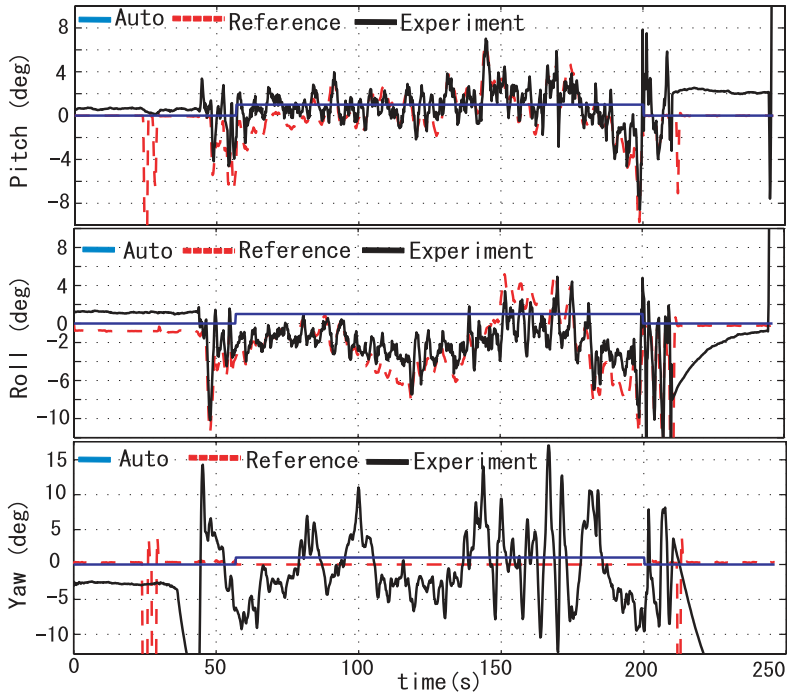

Fig. 9 Quad-rotor Attitude During Autonomous Hovering

The procedure of the experiment was the same as the one used for autonomous hovering. First, the quad-rotor was flown manually. When it was in the field of view of the stereo camera, the quad-rotor was selected as the target and the object tracking process was conducted. Then, the flight was changed from manually to autonomous. After for about 1 minute of autonomous hovering, the quad-rotor was guided to land by applying an altitude reference, which was determined as a function of time of its reference velocity. In our experiment, we applied a constant velocity on the Z direction, 0.4 m/s. The equation for landing process is shown in Eq.(39).

$$h_{ref} = h_{ref} - (\Delta t \cdot v_{h_{ref}}) \tag{39}$$

where h_{ref} is quad-rotor altitude in autonomous hovering mode, Δt is time difference between previous and current data acquisition, and $v_{h_{ref}}$ is velocity reference for autonomous landing.

The experimental setup is shown Fig.2. Here, the stereo vision is placed on a tripod with 45 cm of height. Since the stereo vision can measure the shortest distance for about 25 cm, we applied a strategy that, when quad-rotor is for about 30 cm of distance from stereo vision, we turn off the quad-rotor power automatically, and it will land safely.

X, Y and Z positions of this experiment are shown in Fig.10. As seen in Fig.10(Top) and (Middle), quad-rotor could hover with the accuracy about 0.5 - 1 m along X and Y axis, and about 1 m for Z axis. In case of Z axis, stereo with INS system is compared with pressure sensor. As seen in Fig. 10(Bottom), for Z position, stereo with INS system has better performance compared to pressure sensor. Additionally, quad-rotor MAV could follow the given trajectory accurately for landing purpose, while pressure sensor failed to do so.

The velocities in the X, Y and Z directions are shown in Fig.11. Even though there is slightly difference between velocities from stereo with INS and GPS, but overall the responses are more or less the same, which are 0.4 m/s accuracy for X direction and 0.3 m/s for Y direction. In case of Z direction, the accuracy of the velocity is about 1 m/s.

Fig.12 shows the attitude of quad-rotor MAV during autonomous landing. As we can see here, more or less there are no significant movements in the attitude. The movements of the pitch, roll and yaw angle are about 3°, 3° and 10°, respectively.

These results are as expected since for autonomous landing, the quad-rotor MAV should

have the same attitude in order to maintain the movement only along the Z axis.

6. Conclusion and Future Works

CAMSHIFT algorithm for object tracking was used for quad-rotor tracking. A stereo vision system was used for obtaining accurate world positions of the quad-rotor. By using position information from a stereo vision system, a PID controller for nonlinear model of a quad-rotor, we obtained a reliable result in autonomous hovering and landing.

From the experimental result, it can be seen that the performance of stereo with INS system is better than GPS system. It is obtained that stereo with INS system has accuracy about less than 2 m in height of 6 m, better than GPS, which has accuracy of 5 m in the same height.

These results suggest the possibility of a stereo vision system for precise guidance of an MAV. In the future, such kind of system can be used for many applications, such as automatic battery recharging system, cooperative control among aerial vehicles or among aerial vehicles and ground vehicles.

As for future works, several tasks will be conducted, such as 1) Group control of MAVs with single on ground stereo vision system, 2) Precise positioning using image processing, 3) Autonomous guidance by means of moving on ground stereo vision system, 4) Autonomous guidance and landing by means of moving on ground stereo vision system and 5) Autonomous flight of quad-rotor MAV by an embedded stereo vision system, in order to broaden the range of MAV applications.

Acknowledgement

This research is supported partly by NEC C&C Research Grant for Foreign Researchers in Japan.

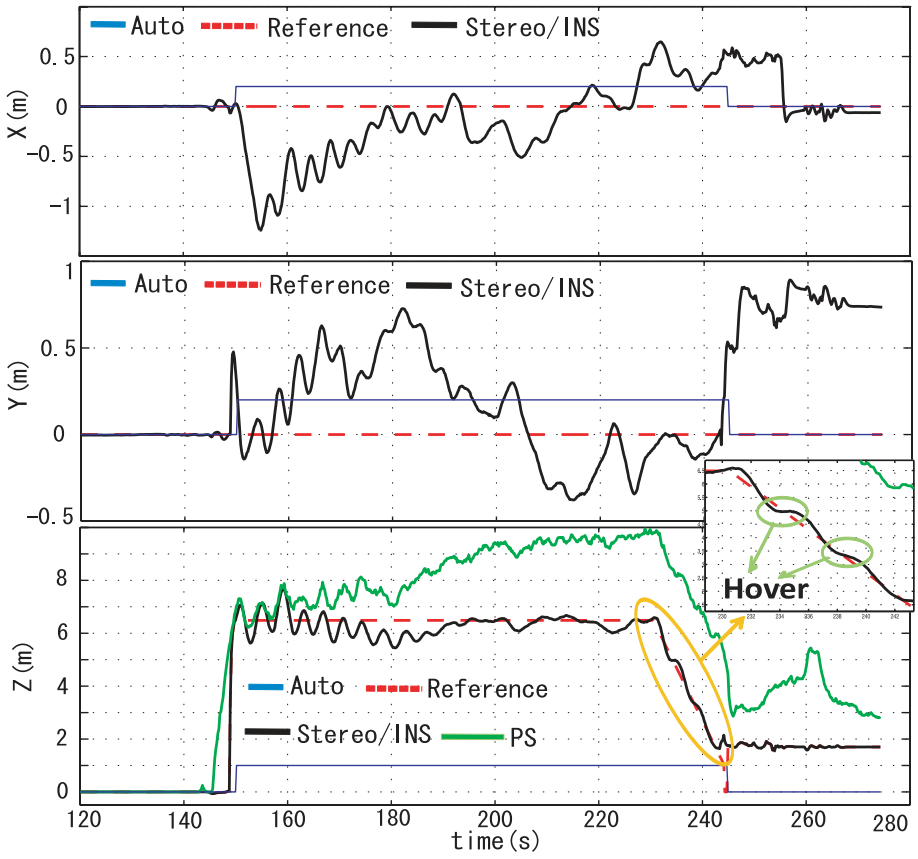

Fig. 10 Quad-rotor Position During Autonomous Landing

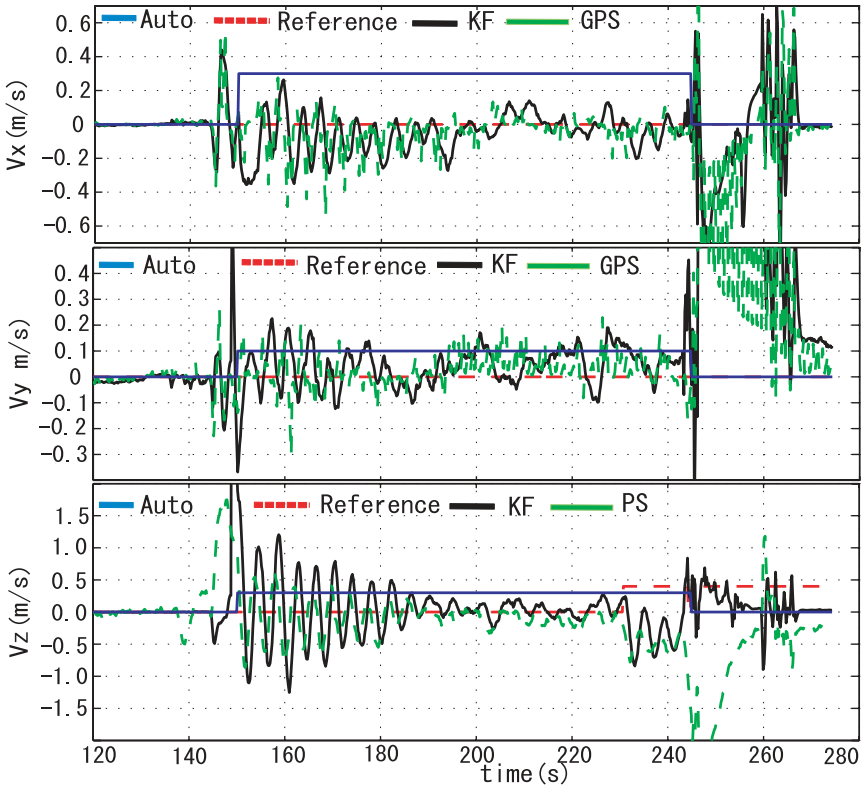

Fig. 11 Quad-rotor Velocities During Autonomous Landing

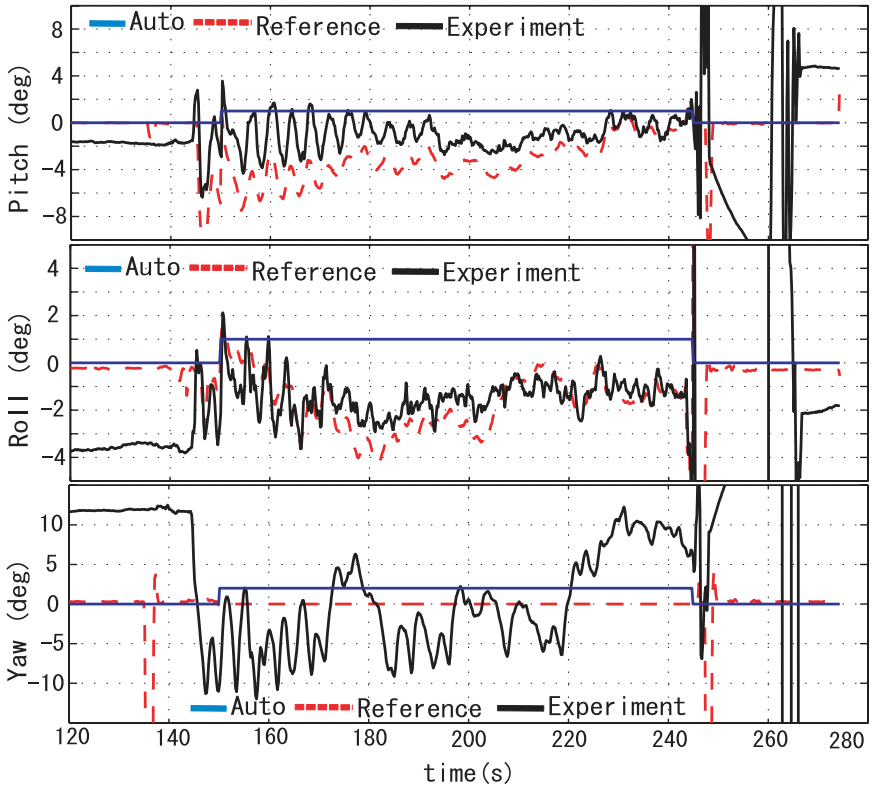

Fig. 12 Quad-rotor Attitude During Autonomous Landing

References

(1) Kendoul, F., "*Modelling and Control of Unmanned Aerial Vehicles and Development of a Vision Based Autopilot for Small Rotorcraft Navigation*", Doctoral Dissertation, 26 September 2007.

(2) Zhen Yu, Demian Celestino, Jinok Shin and Kenzo Nonami, "*3D Vision Based Landing Control of a Small Scale Autonomous Helicopter* ", International Journal of Advanced Robotic System, Vol.4, No.1, 2007.

(3) Srikanth Saripalli, James F. Montgomery and Gaurav S. Sukhatme, "*Vision-based Autonomous Landing of an Unmanned Aerial Vehicle*", IEEE International Conference on Robotics and Automation, May 2002.

(4) Erdinc Altug, James P. Ostrowski, Robert Mahony, "*Control of a Quadrotor Helicopter Using Visual Feedback*" , Proceeding of the 2002 IEEE International Conference on Robotics & Automation, Washington DC, May 2002.

(5) Erdinc Altug, James P. Ostrowski, Camillo J.Taylor, "*Quadrotor Control Using Dual Camera Visual Feedback*", Proceeding of the 2003 IEEE International Conference on Roborics & Automation, Taipei, Taiwan, September 14-19, 2003.

(6) Eric N. Johnson, Alison A. Proctor, Jincheol Ha, and Yoko Watanabe, "*Recent Flight Test Result of Active-Vision Control Systems*", 2005 American Control Conference, Portland OR USA, June 8-10, 2005.

(7) Yuta Oohira, "*Autonomous Swarm Control of Small Indoor Helicopter*", Master Thesis, Chiba University, 2008.

(8) G. Q.Bao, S. S. Xiong, Z. Y. Zhou, " *Vision Based Horizon Extraction for MAV Flight Control*", IEEE Transaction on Instrument & Measurement, Vol.54, No.3, pp. 1067 - 1072, June 2005.

(9) S.M.Ettinger, M. C. Nechyba, P.G. Ifju, M. Waszak, "*Vision-Guided Stability and Control for Micro Aerial Vehicles*", in Proceeding of the 2002 IEEE/RSJ International Conference on Intelligent Robots & System, Switzerland, Oct 2002.

(10) S. Saripalli, G.S. Sukhatne, "*Landing on a Moving Target Using an Autonomous Helicopter*", In Proceeding of The International Conference on Field & Service Robots, Mt. Fuji, Japan, July 2003.

(11) G.R. Bradski, "*Computer Vision Face Tracking for Use in a Perceptual User Interface*", Intel Technology Journal, 2, April-June, 1998.

(12) Intel Corporation, "*Open Source Computer Vision Library Reference Manual*", 123456-001, 2001.

(13) F. Kendoul, I. Fantoni, R. Lozano, "*Asymptotic Stability of Hierarchical Inner-outer Loop-based Flight Controller*", in Proceedigs of the 17th IFAC World Congress, pp. 1741-1746, Seoul, Korea, July 6-11 2008.

(14) P. Castillo, R. Lozano, and A. Dzul. "*Modelling and Control of Mini-Flying Machines.*", Advances in Industrial Control, Springer-Verlag, 2005.

(15) Barnes W. McCormick, "*Aerodynamics, Aeronautics and Flight Mechanics*", John Wiley And Sons, New York, 1995.

(16) Raymond W. Prouty, "*Helicopter Performance, Stability, and Control.*", Krieger Publishing Company, Malabar, Florida, 1995.

(17) F. Kendoul, "Nonlinear Hierarchical Flight Controller for Unmanned Rotorcraft: Design, Stability and Experiments", Engineering Notes, Journal of Guidance, Control and Dynamics, July 2009

(18) Sepulcre, R., Jankovic, M., and Kokotovic, P., "*Constructive Nonlinear Control, Communications and Control Engineering Series*", Springer-Verlag, Berlin/New York/Heidelberg, 1997